**BIO DESIGN**

# Recent advances and future prospects of serial crystallography using XFEL and synchrotron X-ray sources

**Srinivasan Muniyappan**[1,2+], **Seong Ok Kim**[1,2+] **and Hyotcherl Ihee**[1,2*]
[1]Center for Nanomaterials and Chemical Reactions, Institute for Basic Science, Daejeon 305-701, Korea, [2]Department of Chemistry, KAIST, Daejeon 305-701, Korea. *Correspondence: hyotcherl.ihee@kaist.ac.kr
+These authors contributed equally to this work.

Protein structure determination at the atomic level is an essential step for understanding protein functions and developing new drugs. However, growing crystals of sufficient quality and size necessary to obtain good diffraction patterns is a significant bottleneck. The advent of X-ray free electron lasers (XFELs) has made it possible to collect high quality X-ray diffraction patterns from nano- or micro-sized crystals because a typical XFEL pulse is intense enough to provide a diffraction pattern from such small sized crystals and is temporally short (less than 50 femtoseconds) enough to collect the diffraction pattern prior to crystal destruction or significant radiation damage. A combination of this idea and a continuous sample delivery system supplying a fresh crystal for every X-ray pulse provides a nascent field of serial femtosecond crystallography (SFX). The concept of serial crystallography (SX) is also being adapted in conventional micro- and nano-focused synchrotron beamlines, resulting in serial synchrotron crystallography (SSX). In this review, we survey and examine a variety of currently available sample delivery systems in SFX and SSX and discuss their advantages and drawbacks. We also review the protein systems studied by SFX and SSX and various protein crystallization techniques that are particularly useful for membrane proteins in the application with SFX and SSX. Finally, we highlight the applicability of the SFX and SSX methods for time-resolved studies, which offer notable new possibilities for tracking both the reversible and irreversible structural dynamics of proteins at the atomic level in real time. SSX and SFX may revolutionize the field of structural biology.

## INTRODUCTION

The molecular structure of biological macromolecules is of great interest to biologists because macromolecules carry out most of the functions of cells through their specific three-dimensional structures and orchestration among them. To elucidate the relationship between the structure and function of biomolecules, a variety of methods, such as X-ray crystallography (Jaskolski et al., 2014; Richardson and Richardson, 2014; Shi, 2014), nuclear magnetic resonance spectroscopy (Gobl et al., 2014; Osawa et al., 2012; Torchia, 2015), mass spectroscopy (Konermann et al., 2011; Walzthoeni et al., 2013), electron paramagnetic resonance (Duss et al., 2014; Lopez et al., 2014; Mchaourab et al., 2011), cryo-electron microscopy (Bai et al., 2015; Cheng, 2015; Elmlund and Elmlund, 2015) and small angle X-ray scattering (Graewert and Svergun, 2013; Mertens and Svergun, 2010; Petoukhov and Svergun, 2013) have been developed and are being used. These methods provide unprecedented information about the atomic structure, and some of them can even elucidate the dynamics of macromolecules, especially when combined with time-resolved data collection (Ahn et al., 2009; Andersson et al., 2008; Anfinrud et al., 2011; Cammarata et al., 2008; Cho et al., 2010; Cho et al.,

2013; Choi et al., 2008; Choi et al., 2010; Ihee et al., 2005; Jung et al., 2013; Kim et al., 2011; Kim et al., 2012; Kim et al., 2012; Kim et al., 2014; Knapp et al., 2006; Malmerberg et al., 2011; Oang et al., 2014; Oang et al., 2014; Ramachandran et al., 2011).

Among these techniques, X-ray crystallography is one of the most widely used tools. Hence, the brilliance of the third generation synchrotron X-ray beam has contributed greatly to high-resolution crystal structure determination. There are more than 97,000 macromolecular structures that have been determined using synchrotron and other X-ray sources (Berman et al., 2000). However, only a few hundred structures of membrane proteins (MPs) have been determined (Berman et al., 2000; Tusnady et al., 2004) despite the fact that the structures of MPs are essential for novel drug discoveries due to their important roles in signaling pathways as molecular receptors in cells (Venkatakrishnan et al., 2013). The main bottlenecks in membrane protein structural biology are the difficulty in crystallizing and obtaining single crystals of a suitable size for macromolecular crystallographic applications. Moreover, the broad temporal pulse width of synchrotron X-ray beams can lead to radiation damage on single crystals that eventually affect the

integrity of the determined structure (Doniach, 1996). Although it is possible to overcome the radiation damage using cryo-protectants such as glycerol, MPD, ethylene glycol, and low molecular weight PEG, the crystal mosaicity tends to increase substantially when cryo-protection steps are taken (Guha et al., 2012; Malkin and Thorne, 2004).

The fourth generation light source of X-ray Free-Electron Lasers (XFELs) affords a new strategy for solving these problems. XFEL facilitates entirely different approaches in structure determination by providing X-ray pulses that are extremely short (less than 50 femtoseconds) and 10 billion times brighter than any other type of existing X-ray source. This extremely intense femtosecond X-ray pulse ($\sim 10^{12}$ photons/pulse) can be focused to a sub-micrometer focal spot to enable the collection of high quality diffraction data before the destruction of the nano- or micro-sized crystals (Neutze et al., 2000). Radiation damage on small sized crystals at room temperature can be avoided with the aid of a continuous sample delivery system that provides a new fresh crystal for every X-ray pulse. The crystal is eventually damaged or destroyed by the intense X-ray pulse, but the diffraction information is extracted prior to such damage due to the extremely short X-ray pulse width. This method, using a diffract-and-destroy concept, is referred as serial femtosecond crystallography (SFX) (Boutet et al., 2012; Chapman et al., 2011; Spence and Doak, 2004). The SFX data collection scheme is illustrated in Figure 1. Recently, excellent progress has been made with the XFEL beam sources at the Linac Coherent Light Source (LCLS) in the USA (Emma et al., 2010) and at the SPring-8 Angstrom Compact Free-electron Laser (SACLA) in Japan (Ishikawa et al., 2012). This concept of serial crystallography (SX) is also being adapted in synchrotron beamlines equipped with micro- and nano-focused X-ray beams (Schroer et al., 2005) where the diffraction data are obtained from nano- or micro-sized crystals that are streamed or scanned across the X-ray beams using a liquid jet or a fixed-target system. This new approach is termed serial synchrotron crystallography (SSX) (Botha et al., 2015; Coquelle et al., 2015; Gati et al., 2014; Nogly et al., 2015; Rossmann, 2014; Stellato et al., 2014). SFX and SSX may open a new era for resolving the structures of macromolecules such as large sized MPs and complex photosystems.

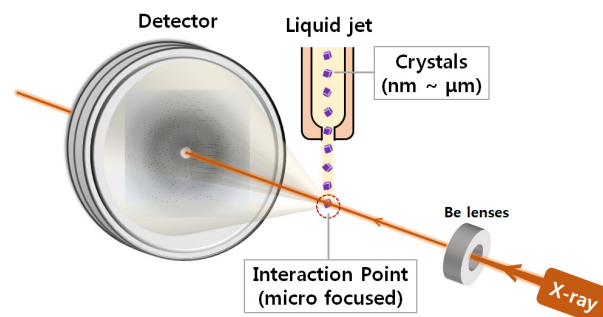In this mini review, we introduce the general features of SFX



**FIGURE 1 ∣ Schematic representation of the SFX experimental setup available at a typical XFEL light source.** Microcrystals are streamed from a liquid jet and intersect with an XFEL beam focused to a few $\mu m^2$ in diameter. The diffraction snapshots are recorded using a detector.

and SSX, discuss the advantages and critical points of currently developed sample delivery systems, outline the proteins studied by these methods, and briefly discuss SX sample preparation processes. Finally, we highlight the time-resolved SFX (TR-SFX) and time-resolved SSX (TR-SSX), which may overcome the drawbacks of time-resolved Laue crystallography and offer notable new possibilities for the monitoring of the structural dynamics of proteins at the atomic level.

## SAMPLE DELIVERY SYSTEMS: FLOW-JET SYSTEMS

The commonly used crystal mounting system is not suitable for SX. For this reason, a variety of sample delivery systems for SX have been reported thus far, and they can be classified as flow-jet systems and fixed-target systems. The sample delivery system should fulfill the following requirements. It should be suitable for crystals of various sizes, covering the $\mu m$ to nm range, be easily adaptable to various types of crystallization methods, provide a continuous sample supply without clogging (in the case of a flow-jet system) or settling (e.g., the sticking of the crystals in a sample reservoir or a flowing tube), and consume minimal amounts of samples with high efficiency. In this section, we first review the flow-jet systems while the next section focuses on fixed targets. Table 1 summarizes the flow-jet systems.

**TABLE 1 ∣** Summary of the SFX sample delivery flow-jet systems

| Flow-jet system | Diameter of the jet (μm) | Flow rate (μl/min) | Sample requirement (mg) | References |
|---|---|---|---|---|
| GDVN injector | 50 | 7 | 10-100* | (Demirci et al., 2013) |
| Electrospun injector | 50 | 0.17–3.1 | 0.14* | (Sierra et al., 2012) |
| LCP injector | 10-50 | 0.003-0.3 | 0.8* | (Liu et al., 2014) |
| Grease matrix assisted syringe | 110 | 0.41-48 | 1* | (Sugahara et al., 2015) |

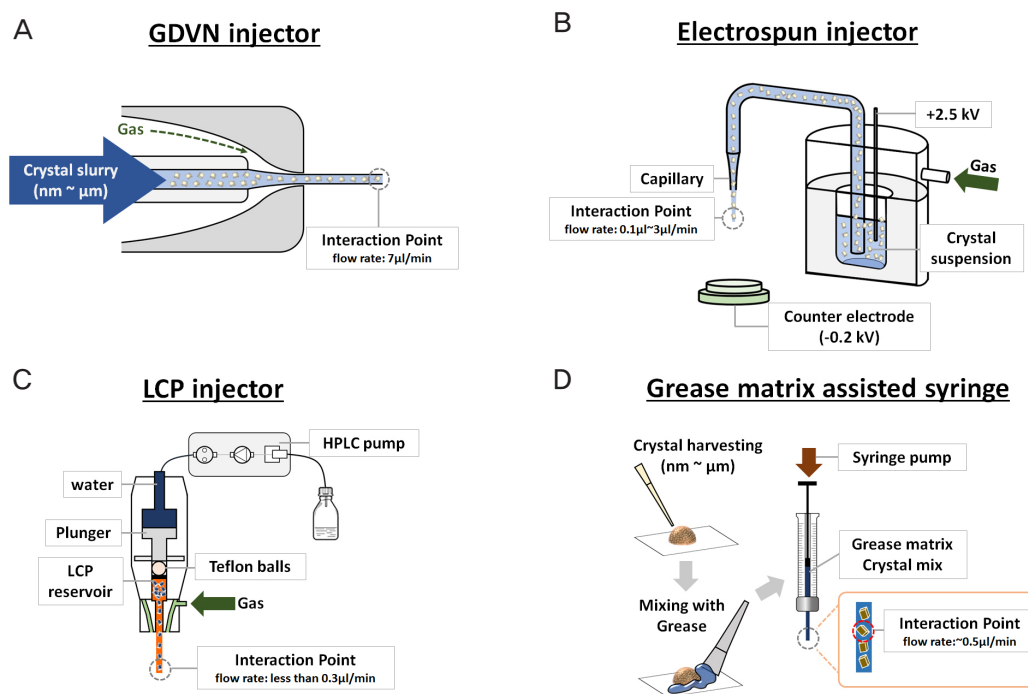* It depends on specific protein samples

**FIGURE 2 | Flow-jet sample delivery systems available for SFX.** (A) The GDVN injector is formed by a buffer containing microcrystals. The sample is injected using an anti-settling injection nozzle. The diameter of the GDVN injector is 50 μm and the flow rate of the crystals is 7 μl/min (Demirci et al., 2013). (B) The electrospun injector. The crystal flow is based on electrospun (electrostatic charging) of the liquid in a vacuum. The diameter of the silica capillary is 50 μm and the flow rate of the crystal is 0.17–3.1 μl/min (Sierra et al., 2012). (C) LCP injector. MP crystals which are grown in LCP media are flowed using a HPLC pump. The diameter of the silica capillary is in the range of 10-50 μm and the flow rate of the crystals ranges from 10 to 300 nl/min (Liu et al., 2014). (D) With a grease matrix assisted syringe, the grown nano- or micro-sized crystals are suspended with mineral oil (grease). The mixture is loaded into a syringe pump and the flow rate of the crystals is ~ 0.5 μl/min (Sugahara et al., 2015).

The first successful SFX sample injector was based on the gas dynamic virtual nozzle (GDVN) injector, which is used to inject microcrystals into an X-ray beam at a flow speed of 10 μl/min (Demirci et al., 2013) (Figure 2A). With this setup and at that flow rate, only 1 out of 10,000 microcrystals is hit by the X-ray pulse with the current X-ray pulse repetition rates of 120 Hz and 60 Hz, respectively, at LCLS and SACLA. The rate of sample consumption is high in the GDVN injector, and it takes 5–6 hours to collect a full data set, which means that more than 10–100 mg of crystal slurry is required to collect a full data set. To overcome the high sample consumption and the rapid flow rate, certain improvements have been made with the GDVN-based electrospun (electrostatic charging) of the liquid in a vacuum (Figure 2B). This modification reduced the flow of the sample to 0.2–3 μl/min (Sierra et al., 2012). However, these types of flow-jet systems require an antifreezing chemical and electrostatic charging, which may be undesirable for some protein crystals.

A further reduction of the sample flow rate is possible with extremely viscous samples such as the lipid cubic phase (LCP). It is also well known that LCP is an excellent crystallization media for MP crystallization. The liquid gel type of LCP medium further reduced the flow of the sample to 10–300 nl/min, which is feasible for use with the 120 Hz X-ray repetition rate at the

LCLS facility (Figure 2C). The LCP medium is a non-Newtonian fluid which does not flow easily. In addition, pressure of about 3,500 psi has to be applied via an attached high-pressure liquid chromatography (HPLC) pump to the LCP medium to reach such flow rates and achieve a continuous sample supply (Liu et al., 2014). Despite the recent successes in the area of LCP injectors with various MP crystals, this method also has a few drawbacks. For instance, the LCP injector works only in a limited temperature range, and the minimal diameter of the capillary nozzle is 10-15 μm, which scatters X-rays and produces a relatively strong background (Liu and Spence, 2014; Liu et al., 2013; Liu et al., 2014).

A more universal method which covers a wide range of protein systems is required. Sugahara et al. developed a new flow system that works in a grease matrix assisted syringe. The grease matrix serves as an excellent carrier for most classes of proteins with a straightforward sample preparation process (Sugahara et al., 2015) (Figure 2D). The grown nano- or micro-sized crystals are suspended with mineral oil (grease) and mixed well using a spatula. The grease matrix containing the microcrystals is then inserted into a pipetting tip. The resulting grease matrix containing the randomly oriented protein microcrystals is loaded into a syringe injector. In their study, the flow rate of the sample

was ~0.5 µl/min and flow was stable during the data collection process.

## SAMPLE DELIVERY SYSTEMS: FIXED-TARGET SYSTEMS

All of the flow-jet systems described thus far require extremely viscous liquid or antifreezing chemicals to reduce the sample consumption and flow rate, which strongly scatter X-ray, resulting in strong background scattering. Moreover, all flow-jet systems require an additional device known as an anti-settling instrument to ensure the smooth flow of crystals and to prevent crystals from settling in the reservoir (Lomb et al., 2012). Fixed-target systems, which are alternative approaches to the flow-jet systems, were developed recently. Fixed-target systems utilize the deposition of crystals on a chip or a grid (Cohen et al., 2014; Hunter et al., 2014; Lyubimov et al., 2015) and on-chip crystallization methods (Dhouib et al., 2009; Gerdts et al., 2008; Guha et al., 2012; Heymann et al., 2014; Khvostichenko et al., 2014; Sauter et al., 2007; Zhu et al., 2014). Table 2 summarizes these systems and Figure 3 shows the fixed-target sample delivery systems. Crystals grown by conventional crystallization methods can be deposited by embedding, trapping on a chip (Hunter et al., 2014; Lyubimov et al., 2015) or by positioning the crystals inside a grid (Cohen et al., 2014) (Figure 3A). These methods enable X-ray diffraction collection with a high hit rate and lower levels of sample consumption (Cohen et al., 2014; Hunter et al., 2014; Lyubimov et al., 2015). However, a drawback of this method is that the crystal deposition step is laborious and time-consuming. In this regard, if both crystallization and diffraction can be done in a single device, it may simplify the sample preparation step. Toward this goal, Dhouib et al. developed a simple and inexpensive microfluidic chip for protein crystallization and demonstrated on-chip crystallization using a counter-diffusion method, such that the same chip can be used for both crystallization and data collection. In this method, the protein solution is injected at one end of the chip and the precipitants are injected at the other end, which creates a gradient of decreasing protein supersaturation and results in a gradual increase of the crystal size on the chip (Figure 3B). This method requires less of the protein sample (~150 nl), and the crystal diffraction quality is modest (2.8 Å) (Dhouib et al., 2009). The maximum supersaturation varies along the channel (capillary) length. A drawback of this method is that the number of crystals is generally limited and to generate more than a thousand crystals, this method requires long channels (capillaries). Therefore, an alternative method that can contain a larger number of crystals in a single chip was desired. Heymann et al. demonstrated an emulsion droplets-based high-throughput crystallization approach. With this method, monodisperse emulsions are prepared by flowing protein, oil and the precipitant onto a dedicated drop-making chip, which creates drops of a desired diameter (Figure 3C). The formation of one crystal per drop is based on competition between nucleation and growth. Using this method, thousands of suitably diffractive micro-crystals can be grown in the X-ray semi-transparent microchips. The crystals grown or deposited in the microchips can be mounted directly onto goniometer or a moving stage, which can be moved orthogonally to the beam path, and the diffraction data can be collected serially from the crystals (Cohen et al., 2014; Dhouib et al., 2009; Gerdts et al., 2008; Guha et al., 2012; Heymann et al., 2014; Hirata et al., 2014; Hunter et al., 2014; Khvostichenko et al., 2014; Kisselman et al., 2011; Sauter et al., 2007; Zhu et al., 2014) (Figure 3D). The chip- or grid-based fixed-target system can be used even with third generation synchrotron sources. The rapid development of flow-jet and fixed-target systems may provide a technological breakthrough in the SFX and SSX data collection methodology.

## DATA ANALYSIS AND PROTEIN SYSTEMS STUDIED BY SERIAL CRYSTALLOGRAPHY

Unlike conventional crystallography, serial crystallography involves additional data processing steps prior to the structure determination process due to its data collection strategy. All diffraction patterns come from randomly oriented crystals and are not correlated because the crystals are randomly suspended or embedded, respectively, in a flow-jet system and a fixed-

**TABLE 2** | Summary of the SFX fixed-target sample delivery system

| Preparation of the fixed-target system | Dimensions of the device | Materials used for device fabrication | Sample requirement | References |
|---|---|---|---|---|
| Crystal embedding in a chip | ~16.8 mm × 6.4 mm | $Si_3N_4$ membranes | 540 µg | (Hunter et al., 2014) |
| Crystal trapping in a chip | ~10 mm × 25 mm | PDMS, PMMA | < 5 µl | (Lyubimov et al., 2015) |
| Crystal positioning inside a grid | 18.5 mm × 2.7 mm | Polycarbonate plastic | Not given | (Cohen et al., 2014) |
| On-chip crystallization (counter-diffusion) | ~45 mm × 45 mm | PDMS, PMMA and COC | ~ 150 nl | (Dhouib et al., 2009) |
| On-chip crystallization (emulsion droplets) | 2.36 mm × 3.36 mm | PDMS | ~ 0.8 µl  (<1 nl/drop) | (Heymann et al., 2014) |

Abbreviation: PDMS, Poly(dimethylsiloxane); PMMA, Poly-methyl-methacrylate; COC, Cyclo-olefin-copolymer.
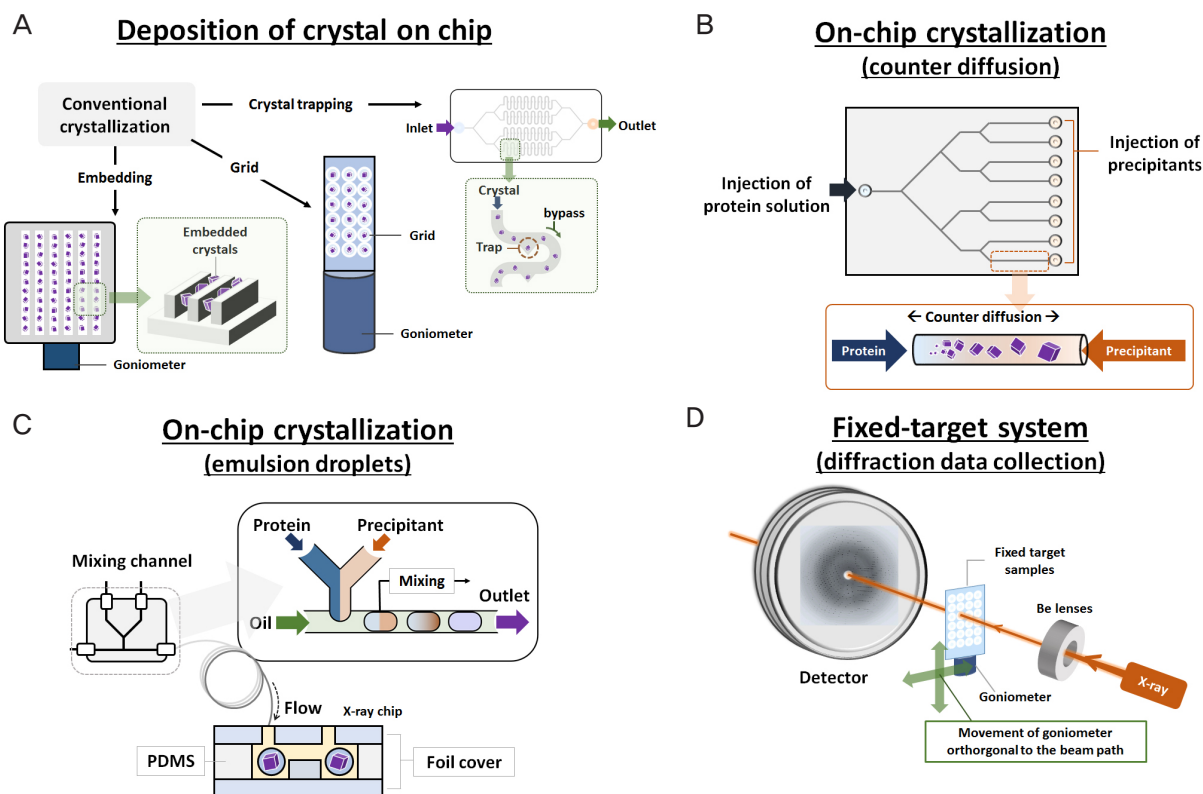
**FIGURE 3 | Sample preparation for fixed-target systems and diffraction data collection.** (A) Deposition of crystals on a chip or a grid. The crystals are prepared by conventional crystallization methods. The crystals are deposited by embedding, trapping them on a chip, or by positioning the crystals inside a grid. (B) On-chip crystallization based on counter–diffusion. The protein solution is injected from one end. On the other end, precipitants will be loaded to create a gradient of decreasing protein supersaturation that results in a gradual increase of the crystal size (Dhouib et al., 2009). (C) On-chip crystallization based on emulsion droplets. Monodisperse emulsions were prepared by flowing protein, precipitant and oil in to a dedicated drop-making chip, which creates drops with a desired diameter. The crystals are grown in an X-ray semi-transparent microfluidic chip (Heymann et al., 2014). (D) The fixed-target system diffraction data collection. The X-ray semi-transparent microfluidic chip is mounted on a goniometer which moves orthogonally to the X-ray beam path and collects the diffraction data.

target system at a sample delivery stage. A large percentage of the image frames also may contain empty hits or multi-crystal hits, depending on the type of the sample delivery system, the concentration of the crystals, and the X-ray pulse repetition rate. SX generally collects partially integrated Bragg reflections because oscillation or rotation during X-ray exposure is generally not possible. Moreover, SX uses a high X-ray pulse repetition rate (60 Hz at SACLA and 120 Hz at LCLS) producing 3,600 and 7,200 image frames per minute, which means that tens of thousands of image frames need to be processed for a single data set. Therefore, high throughput automated processing is important for producing a manageable and useful data set for structure determination from an enormous data set. The first step of data analysis focuses on the identification of useful diffraction patterns, which is called 'hit finding', among the SX data set. This step can be performed using the programs Cheetah (Barty et al., 2014) or CASS (Foucar et al., 2012) by judging the typical number of Bragg peaks in the image frames. Next, serial diffraction data can be analyzed by CrystFEL (White et al., 2012; White et al., 2013), cctbs.xfel (Hattne et al., 2014) or

nXDS (Kabsch, 2014). These programs identify Bragg peaks in the hits, and pass lists of reflections for the indexing, integrating and merging of the partial diffraction intensities. One of the critical drawbacks of the SX data analysis is the requirement of phase retrieval from recorded diffraction data. Thus far, only the molecular replacement phase retrieval procedure has been used to solve the structure by SX. This method limits the target protein molecules amendable to SX because the protein of interest should have a homologous crystal structure to retrieve the phase information. New phase retrieval methods are desired in order to expand the applicability of SX. Currently, new phasing methods have been proposed for SFX data analysis, such as direct phasing using inter-Bragg intensities from SFX diffraction data (Chapman et al., 2011) and phase retrieval using conventional multi- or single-wavelength anomalous diffraction (MAD or SAD) methods (Barends et al., 2013; Barends et al., 2014; Son et al., 2011; Son et al., 2013). In direct phasing, the phase is retrieved using the fringes between neighboring Bragg peaks recorded from the nano- or micro-crystals. Each recorded Bragg peak represents a particular portion of the Ewald sphere and phasing

is achieved by oversampling between the Bragg peaks. This method was successfully applied to retrieve the phase from SFX data of photosystem II (Chapman et al., 2011). Recently, the conventional multi- or single-wavelength anomalous diffraction (MAD or SAD) methods are also being adapted for SFX phase retrieval. Barends et al. demonstrated a *de novo* phasing by analyzing a single-wavelength anomalous dispersion (SAD) signal from SFX diffraction data of gadoteridol-treated lysozyme and retrieved phase information without any prior knowledge about the protein structure (Barends et al., 2014). Currently, the MAD phasing method is also adapted to SFX diffraction data using modified Karle–Hendrickson equations (Son et al., 2011; Son et al., 2013).

Despite the current limitations with the phase retrieval process, the SX method has been successfully applied to various protein systems, and their structures have been solved at high resolutions. Tables 3 and 4 summarize the various protein systems studied using SSX and SFX, respectively.

## SAMPLE PREPARATION FOR SERIAL CRYSTALLOGRAPHY

As mentioned previously, preparing protein crystals remains challenging even for SX because the crystallization success rates are based on a number of different parameters and require many iteration cycles. Moreover, it is essential to grow large numbers of well-ordered and well-diffracting nano- or micro-crystals for successful SFX and SSX experiments. Although several conventional protein crystallization techniques are available, here we provide a brief overview of only the lipid-based and free interface diffusion crystallization methods because these crystallization methods enhance the applicability of SFX and SSX methods for the following reasons. The lipid medium supports

a slow flow rate of the liquid jet with less sample consumption and helps with the growth of the MP crystals. Crystals grown using a lipid medium can be loaded directly into the liquid jets. In fact, even crystals grown using conventional techniques can be mixed with a lipid medium and flowed using a liquid jet to avoid the sample wastage problem (Botha et al., 2015; Liu et al., 2014). In recent years, a number of challenging MP targets were crystallized using advanced lipid-based methods such as the lipidic cubic phase (LCP) (Cherezov et al., 2004; Cherezov et al., 2007), lipidic sponge phase (LSP) (Wadsten et al., 2006; Wohri et al., 2008) and lipidic bicelle crystallization methods (Faham and Bowie, 2002; Rasmussen et al., 2007). These lipidic phase crystallization approaches are emerging as powerful complementary crystallization methods for MP that can be used with SFX and SSX (Botha et al., 2015; Liu et al., 2014; Nogly et al., 2015).

The LCP method uses the protein/lipid mixture, i.e., a LCP matrix, which creates a membrane-like environment and supports the growth of MP crystals. The formation of the LCP matrix is based on a monoolein-water phase diagram. MP in LCP can be achieved with a 60:40 (w/w) lipid-cholesterol mixture with the MP reconstituted within a minute (Ghosh et al., 2015). For a high-throughput screen, the LCP method can be automated by a crystallization robot (Cherezov et al., 2004) and the crystalized MP in LCP can be directly used with the SFX and SSX in an LCP injector (Liu et al., 2014; Nogly et al., 2015). Bacteriorhodopsin was the first MP successfully crystallized using the LCP method (PebayPeyroula et al., 1997). More than 11% of currently deposited structures of MP in PDB have been crystallized using the LCP method (Cherezov, 2011).

Another widely used approach for MP crystallization is the LSP method. It is derived from LCP by the addition of a third

**TABLE 3** | Summary of the various protein systems studied by SSX

| Protein name | Light source | X-ray energy (keV) | Sample delivery system | Resolution (A°) | References |
|---|---|---|---|---|---|
| Lysozyme | PXII at SLS | 9.4 | LCP injector[a] | 2.30–2.17 | (Botha et al., 2015) |
| Bacteriorhodopsin | ID13 at ESRF | 13 | LCP injector | 2.46–2.40 | (Nogly et al., 2015) |
| Lysozyme | 12-2 at SSRL | Not given | Fixed-target (crystal trapping in a chip) | 2.5 | (Lyubimov et al., 2015) |
| Lysozyme | ID13 at ESRF | 13 and14 | Fixed-target (grid) | 2.05–1.7 | (Coquelle et al., 2015) |
| Procathepsin B | PETRA III at DESY | 10 | Fixed-target (grid)[b] | 3 | (Gati et al., 2014) |
| Glucose isomerase | F1 at CHESS | 13.5 | Fixed-target (on-chip crystallization)[c] | 2.09 | (Heymann et al., 2014) |
| Lysozyme | PETRA III at DESY | 9.8 | GVDN injector | 2.1 | (Stellato et al., 2014) |
| Pol II–TFIIB–NAS | BL12-2 at SSRL | Not given | Fixed-target (grid) | 3.3 | (Cohen et al., 2014) |
| Thaumatin | FIP-BM30A at ESRF | 12.6 and 8 | Fixed-target (on-chip crystallization)[d] | 2.8 | (Dhouib et al., 2009) |

[a]LCP injector (high-viscosity extrusion injector). [b]A nylon loop was used as a grid. [c]The emulsion droplets method was used for on-chip crystallization. [d]The counter diffusion method was used for on-chip crystallization.

component, polyethylene glycol (PEG), which swells the LCP medium to form an LSP (Wohri et al., 2009). The swelling process increases the aqueous pore diameter such that it becomes three times larger than that formed by the LCP method, resulting in sufficient room for the incorporation of MPs with a high content of hydrophilic domains (Cherezov et al., 2007; Wadsten et al., 2006). LSP has the following advantages over LCP. The LSP method can be easily applied in a continuous flow system in a SFX experiment due to the liquid nature of the materials, with low viscosity, whereas the LCP method cannot be applied to a fast flow system due to the semisolid toothpaste-like nature of the materials (Cherezov et al., 2007; Wadsten et al., 2006; Wohri et al., 2009). Recently, Wohri et al. reported that they successfully crystalized eight MPs out of eleven using the LSP method (Wohri et al., 2008). One of the critical disadvantages of the LCP and LSP methods is that both can be used only at room temperature; below 20ºC, both the LCP and LSP matrices turn into the solid lamellar crystal phase, which is not suitable for MP crystallization

purposes (Cherezov et al., 2001).

In the bicelle crystallization approach, the bicelles are achieved by mixing DMPC (1,2-dimyristoyl-sn-glycero-3-phosphocholine) and CHAPSO (3-[3-cholamidopropyl]dimethyl-ammonio)-hydroxy-1-propanesulfonate), after which the mixture is subjected to cycles of vortexing, heating and cooling on ice to form a homogenous bicelle liquid. Then, MPs are mixed with the bicelle liquid, vortexed, and incubated on ice for the insertion of MPs into the bicelle. The incorporation of the MPs into the bicelle liquid can be carried out at 4ºC, and a gel forms above room temperature (20ºC-37ºC) which is a good condition for crystallization to occur. Therefore, the bicelle crystallization method slightly covers the drawback of the LCP and LSP methods.

With these three methods, a variety of MPs and photosystems have been crystalized (Misquitta et al., 2004; Ogata and Lubitz, 2014; PebayPeyroula et al., 1997; Rasmussen et al., 2007; Redecke et al., 2013; Wadsten et al., 2006; Weierstall et al.,

**TABLE 4** | Summary of the various protein systems studied by SFX

| Protein name | Light source | X-ray energy (keV) | Sample delivery system | Resolution (A°) | References |
|---|---|---|---|---|---|
| Lysozyme | BL3 at SACLA | 10 | GVDN injector[a]<br>GVDN injector | 2.44-2.40<br>2.49-2.40 | (Tono et al., 2015) |
| Lysozyme | SACLA | 10 | Grease matrix assisted syringe | 2 | (Sugahara et al., 2015) |
| Glucose isomerase | SACLA | 10 | Grease matrix assisted syringe | 2 | (Sugahara et al., 2015) |
| Thaumatin I | SACLA | 10 | Grease matrix assisted syringe | 2 | (Sugahara et al., 2015) |
| FABP3 | SACLA | 10 | Grease matrix assisted syringe | 1.6 | (Sugahara et al., 2015) |
| Pol II–TFIIB–NAS | CXI at LCLS<br>XPP at LCLS | 9.6<br>Not given | GDVN injector<br>Fixed-target (grid) | 4.0<br>3.7 | (Cohen et al., 2014) |
| CpI [FeFe]-hydrogenase | XPP at LCLS | Not given | Fixed-target (grid) | 1.62–1.60 | (Cohen et al., 2014) |
| Myoglobin | XPP at LCLS | Not given | Fixed-target (grid) | 1.4–1.36 | (Cohen et al., 2014) |
| PYP | CXI at LCLS | 9 | GVDN injector | 1.8 | (Tenboer et al., 2014) |
| Cry3A | CXI at LCLS | 8.52 | GVDN injector | 2.9 | (Sawaya et al., 2014) |
| REP24 | CXI at LCLS | 8 | Fixed-target (crystal embedding in a chip) | 2.5 | (Hunter et al., 2014) |
| Photosystem II | CXI at LCLS | 6.0 | GVDN injector | 5.5 | (Kupitz et al., 2014) |
| SMO/cyclopamine | CXI at LCLS | 9.5 | LCP injector | 3.2 | (Weierstall et al., 2014) |
| TbCatB | CXI at LCLS | 9.4 | GVDN injector (liquid microjet) | 2.1 | (Redecke et al., 2013) |
| RC$_{vir}$ | CXI at LCLS | 8.8 | GVDN injector (injector nozzle) | 2.8 | (Johansson et al., 2013) |
| 30S ribosomal subunit | CXI at LCLS | 8.5 | GVDN injector | >6 | (Demirci et al., 2013) |
| Photosystem II | CXI at LCLS | 7 and 9 | Electrospun injector | 5.7 | (Kern et al., 2013) |
| Lysozyme | CXI at LCLS | 9.4 | GVDN injector (liquid microjet) | 1.9 | (Boutet et al., 2012) |
| Photosystem II | CXI at LCLS | 9 | Electrospun injector | 6.5 | (Kern et al., 2012) |
| TbCatB | LCLS | 2 | GVDN injector (liquid microjet) | 7.5 | (Koopmann et al., 2012) |
| Photosystem I | LCLS | 1.8 | GVDN injector (liquid microjet) | 8.5 | (Chapman et al., 2011) |

[a]Liquid-jet injector with a sample circulator

2014; Wohri et al., 2009), yielding suitably diffractive nano- or micro-sized crystals (Redecke et al., 2013; Weierstall et al., 2014). Along with lipidic phase methods, batch and free interface diffusion (FID) methods are also used for the production of nano- or micro-sized crystals which are suitable for SFX. In the FID method, the crystals are grown at the interface between a highly concentrated protein solution and a precipitant solution. The protein solution is carefully layered on top of the precipitant solution, such as at 15% PEG2000 (Kupitz et al., 2014). The advantage of the FID method is that the size of grown crystals is significantly smaller with an average radius of 0.5–2 µm, which is suitable for flowing in the jet system (the diameter of the jet is 0.3-20 µm) (Weierstall et al., 2012). Moreover, it is possible to control the size of the crystals and the rate of crystallization by varying the nucleation time from 30 minutes to 24 hours. The crystallization techniques discussed here have been verified on various protein systems and meet the sample demands of SFX and SSX (Kupitz et al., 2014; Misquitta et al., 2004; Ogata and Lubitz, 2014; PebayPeyroula et al., 1997; Rasmussen et al., 2007; Redecke et al., 2013; Wadsten et al., 2006; Weierstall et al., 2014; Wohri et al., 2009).

## TIME-RESOLVED STUDIES USING SFX AND SSX

Proteins are not static in terms of their structure, and a functioning protein spans a rather large area of the structural phase space. Therefore, to understand the function of a protein, it is important to probe its time-dependent molecular motions and reaction intermediates at the atomic level. Over the past several decades, various time-resolved spectroscopic tools have been applied to probe the molecular motions involved in chemical reactions. However, time-resolved spectroscopic tools can extract rather limited structural information because they are sensitive to only chromophore regions or specific energy states of an intermediate. These limitations can be overcome by X-ray based time-resolved structural probes such as time-resolved X-ray liquidography (TRXL) and time-resolved X-ray Laue crystallography. TRXL is an excellent tool for tracking protein motions and reaction intermediates because the TRXL measurements can be performed in the native aqueous state environment without the need of the sample crystallization. Using TRXL, the structural dynamics of various small molecules (Ihee, 2009; Ihee et al., 2010; Kim et al., 2012; Kim et al., 2013; Kim et al., 2013; Kim et al., 2015; Kim et al., 2009; Kong et al., 2005; Kong et al., 2008; Kong et al., 2010; Lee et al., 2013) and biomolecules (Ahn et al., 2009; Andersson et al., 2008; Cho et al., 2010; Cho et al., 2013; Kim et al., 2012; Kim et al., 2012; Kim et al., 2014; Malmerberg et al., 2011; Oang et al., 2014; Oang et al., 2014) were studied with a high spatiotemporal resolution. In a solution, protein molecules are in random orientation. Therefore their scattering patterns are obtained as the average scattering response from those randomly oriented molecules. Thus, this spatial averaging (isotropic average) leads to a loss of information content in the scattering patterns as compared with the diffraction patterns from crystalline samples.

In this regard, time-resolved X-ray Laue crystallography provides unprecedented structural information about reaction intermediates with a high spatiotemporal resolution and without a loss of information. In fact, time-resolved Laue crystallography can be considered as a prior version of serial crystallography, in the sense that a small portion of a large protein crystal is irradiated with a laser pulse and a diffraction pattern is then collected by an X-ray probe pulse at a specific time delay, and this pump-probe cycle of data collection is serially conducted with spatial translation of the crystal to avoid the accumulation of crystal damage (Ihee et al., 2005; Schmidt et al., 2005). Using time-resolved Laue crystallography, the ultrafast dynamics of many protein systems have been studied (Anfinrud et al., 2011; Bilderback et al., 1984; Blum et al., 1990; Genick et al., 1997; Ihee et al., 2005; Jung et al., 2013; Knapp et al., 2006; Ng et al., 1993; Schmidt et al., 2004; Schotte et al., 2012; Srajer et al., 1996; Srajer et al., 2001). This technique generally requires a well diffracting crystal of a large size, and a series of time-resolved diffraction patterns must be obtained from a single crystal. For these reasons, the application of time-resolved Laue crystallography has been limited to a few model systems with a reversible photocycle.

Time-resolved X-ray serial crystallography has the potential to remove such limitations because the crystal is replenished for every X-ray shot, which allows one to track irreversible reactions and opens the way to the study of the dynamics of various protein systems at the atomic level. For this reason, the time-resolved serial crystallography method is evolving and is viewed as a tool complementary to conventional time-resolved Laue crystallography. The XFEL light sources at LCLS and SACLA are equipped with a laser set-up for studying the time-resolved dynamics of proteins and small molecules. The time resolution is generally dictated by the X-ray pulse width, and the femtosecond X-rays from XFELs will improve the time resolution down to tens of femtoseconds from the ~100 ps width available in third generation synchrotron light sources. The femtosecond time resolution has been already achieved and demonstrated for time-resolved X-ray liquidography (solution scattering) at XFELs, and the ultrafast dynamic processes of various chemical and biological molecules have been studied (Arnlund et al., 2014; Kim et al., 2015; Lemke et al., 2013; Levantino et al., 2015; Zhang et al., 2014). For example, ultrafast reactions such as bond formation and breaking in the Au oligomer complex were recently tracked successfully by time-resolved X-ray solution scattering with a sub-picosecond time resolution and a sub-angstrom spatial resolution (Kim et al., 2015).

The experimental scheme of time-resolved serial femtosecond crystallography (TR-SFX) is fundamentally identical to a typical time-resolved experiment and requires a reaction initiation process such as photoexcitation, as illustrated in Figure 4. The reaction can be initiated in various ways, including mixing with substrates or via a temperature jump, a pressure
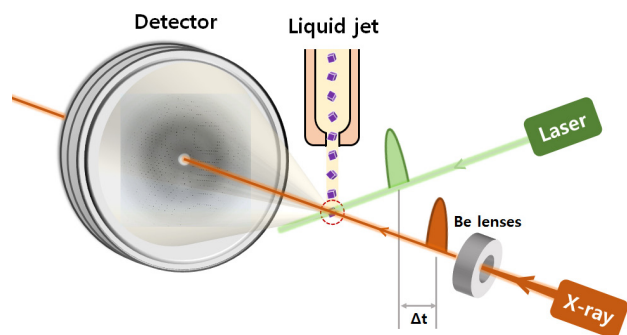
**FIGURE 4 | Schematic representation of the TR-SFX setup available at the XFEL light source.** Randomly oriented crystals are flowed in the path of the X-ray beam using liquid jets. The crystals are triggered by an optical laser pulse before interacting with the femtosecond X-ray FEL pulses.

jump, an electric field, and through irradiation. Among these, photoexcitation provides the best time resolution but requires that the protein of interest should respond to irradiation. Kupitz et al. studied the dynamics of Photosystem II using TR-SFX. They were able to track the light-driven water splitting process and $O_2$ evolution with a microsecond time resolution. However, atomic level interpretations of the structural changes remain ambiguous owing to the limited spatial resolution (Kupitz et al., 2014; Redecke et al., 2013). Tenboe et al. improved the time resolution of TR-SFX to nanosecond time resolution and studied the ultrafast dynamics of photoactive yellow protein (PYP). Their results allowed the determination of the structures of the reaction intermediates which form between ~200 ns and 100 µs at an atomic resolution (1.6 Å). However, the sub-picosecond structural dynamics of various photoreceptors and heme proteins such as blue-light sensors using flavin adenine dinucleotide (BLUF), phytochromes, light-oxygen-voltage (LOV) sensors, cryptochromes, rhodopsins, hemoglobin, myoglobin and cytochrome c have yet to be investigated at the atomic resolution (Bourgeois et al., 2006; Jung et al., 2013; Kern et al., 2013; Knapp et al., 2006; Kupitz et al., 2014; Schotte et al., 2012; Tenboer et al., 2014). The TR-SFX and TR-SSX methods may open up a new era of the study of the ultrafast and slow dynamics of these different photoreceptors and their signaling properties at atomic resolutions.

Recently, it has been proposed that time-resolved crystallographic experiments are possible through the mixing of a substrate with nanocrystals (Schmidt, 2013). Double-focusing mixing jets have been developed to monitor the reversible and irreversible biochemical reactions with rapid mixing and an adjustable delay time (Wang et al., 2014). Thus, the technological advances related to mixing jets will allow us to monitor pharmaceutically important enzymatic reactions by the mixing of nano- or micro-sized protein crystals of interest with small molecules or virtually designed drugs. Tracking the atomic level dynamics of macromolecules such as photoreceptors and

membrane receptors using TR-SFX and TR-SSX will enhance our understanding of the dynamic nature of biomacromolecules and facilitates the subsequent design of novel optogenetics tools, nano-sized molecular machines, and drugs.

## CONCLUDING REMARKS

Despite the recent successes related to SFX and SSX, many technical challenges remain to be resolved before these techniques can be developed as general tools for the study of the structural dynamics of biomolecules. One of the critical challenges is to improve the sample delivery system to minimize sample consumption, decrease clogging, and minimize the settling of crystals in the reservoir. New approaches are required for the phasing and indexing of diffraction data. Each collected diffraction pattern contains a strong background scattering of water ring from the liquid jet, and this water ring makes it difficult to index the diffraction data. The development of new sample delivery systems which minimizes this background scattering is strongly desired in relation to SFX and SSX. Soon, superconducting linac-based XFELs will be operated with a repetition rate of 1 MHz. This will reduce the sample waste problem in SFX. The commissioning of new XFELs such as PAL-XFEL in South Korea, the European XFEL in Germany, SwissFEL in Switzerland, and SINAP XFEL in China will open a new gateway for the structural biology field. In conclusion, serial crystallography at a fast-growing number of successful XFELs and synchrotron light sources will occupy and fulfill the dreams of many structural biologists in the coming decades.

### AUTHOR INFORMATION

The authors declare no potential conflicts of interest

### REFERENCES

Ahn, S., Kim, K.H., Kim, Y., Kim, J., and Ihee, H. (2009). Protein tertiary structural changes visualized by time-resolved X-ray solution scattering. *J Phys Chem B* **113**, 13131-13133.

Andersson, M., van der Spoel, D., Davidsson, J., and Neutze, R. (2008). A proposed time-resolved X-ray scattering approach to track local and global conformational changes in membrane transport proteins. *Structure* **16**, 21-28.

Anfinrud, P., Schotte, F., Cho, H.S., Dashdorj, N., Royer, W., Soman, J., and Olson, J. (2011). Using X-rays to watch proteins function with 100 picosecond time resolution. *Biophys J* **100**, 222-223.

Arnlund, D., Johansson, L.C., Wickstrand, C., Barty, A., Williams, G.J., Malmerberg, E., Davidsson, J., Milathianaki, D., DePonte, D.P., Shoeman, R.L., Wang, D.J., James, D., Katona, G., Westenhoff, S., White, T.A., et al. (2014). Visualizing a protein quake with time-resolved X-ray scattering at a free-electron laser. *Nat Methods* **11**, 923-926.

Bai, X.C., McMullan, G., and Scheres, S.H.W. (2015). How cryo-EM is revolutionizing structural biology. *Trends Biochem Sci* **40**, 49-57.

Barends, T.R., Foucar, L., Shoeman, R.L., Bari, S., Epp, S.W., Hartmann, R., Hauser, G., Huth, M., Kieser, C., Lomb, L., Motomura, K., Nagaya, K., Schmidt, C., Strecker, R., Anielski, D., et al. (2013). Anomalous signal from S atoms in protein crystallographic data from an X-ray free-electron laser. *Acta Crystallogr D Biol Crystallogr* **69**, 838-842.

Barends, T.R., Foucar, L., Botha, S., Doak, R.B., Shoeman, R.L., Nass, K., Koglin, J.E., Williams, G.J., Boutet, S., Messerschmidt, M., and Schlichting, I. (2014). De novo protein crystal structure determination from X-ray free-electron laser data. *Nature* **505**, 244-247.

Barty, A., Kirian, R.A., Maia, F.R.N.C., Hantke, M., Yoon, C.H., White, T.A., and Chapman, H. (2014). Cheetah: software for high-throughput reduction and analysis of serial femtosecond X-ray diffraction data. *J Appl Crystallogr* **47**, 1118-1131.

Berman, H.M., Westbrook, J., Feng, Z., Gilliland, G., Bhat, T.N., Weissig, H., Shindyalov, I.N., and Bourne, P.E. (2000). The Protein Data Bank. *Nucleic Acids Res* **28**, 235-242.

Bilderback, D.H., Moffat, K., and Szebenyi, D.M.E. (1984). Time-Resolved Laue Diffraction from Protein Crystals-Instrumental Considerations. *Nucl Instrum Meth A* **222**, 245-251.

Blum, E.B., Chen, Y., Moffat, K., and Teng, T.Y. (1990). Time-Resolved X-Ray Crystallography of Photoactive Yellow Protein. *Biophys J* **57**, A422-A422.

Botha, S., Nass, K., Barends, T.R., Kabsch, W., Latz, B., Dworkowski, F., Foucar, L., Panepucci, E., Wang, M., Shoeman, R.L., Schlichting, I., and Doak, R.B. (2015). Room-temperature serial crystallography at synchrotron X-ray sources using slowly flowing free-standing high-viscosity microstreams. *Acta Crystallogr D Biol Crystallogr* **71**, 387-397.

Bourgeois, D., Vallone, B., Arcovito, A., Sciara, G., Schotte, F., Anfinrud, P.A., and Brunori, M. (2006). Extended subnanosecond structural dynamics of myoglobin revealed by Laue crystallography. *Proc Natl Acad Sci USA* **103**, 4924-4929.

Boutet, S., Lomb, L., Williams, G.J., Barends, T.R., Aquila, A., Doak, R.B., Weierstall, U., DePonte, D.P., Steinbrener, J., Shoeman, R.L., Messerschmidt, M., Barty, A., White, T. A., Kassemeyer, S., Kirian, R.A., et al. (2012). High-resolution protein structure determination by serial femtosecond crystallography. *Science* **337**, 362-364.

Cammarata, M., Levantino, M., Schotte, F., Anfinrud, P.A., Ewald, F., Choi, J., Cupane, A., Wulff, M., and Ihee, H. (2008). Tracking the structural dynamics of proteins in solution using time-resolved wide-angle X-ray scattering. *Nat Methods* **5**, 881-886.

Chapman, H.N., Fromme, P., Barty, A., White, T.A., Kirian, R.A., Aquila, A., Hunter, M.S., Schulz, J., DePonte, D.P., Weierstall, U., Doak, R.B., Maia, F.R.N.C., Martin, A.V., Schlichting, I., Lomb, L., et al. (2011). Femtosecond X-ray protein nanocrystallography. *Nature* **470**, 73-77.

Cheng, Y. (2015). Single-Particle Cryo-EM at Crystallographic Resolution. *Cell* **161**, 450-457.

Cherezov, V., Fersi, H., and Caffrey, M. (2001). Crystallization screens: Compatibility with the lipidic cubic phase for in meso crystallization of membrane proteins. *Biophys J* **81**, 225-242.

Cherezov, V., Peddi, A., Muthusubramaniam, L., Zheng, Y.F., and Caffrey, M. (2004). A robotic system for crystallizing membrane and soluble proteins in lipidic mesophases. *Acta Crystallogr D Biol Crystallogr* **60**, 1795-1807.

Cherezov, V., Rosenbaum, D.M., Hanson, M.A., Rasmussen, S.G.F., Thian, F.S., Kobilka, T.S., Choi, H.J., Kuhn, P., Weis, W.I., Kobilka, B.K., and Stevens, R.C. (2007). High-resolution crystal structure of an engineered human beta(2)-adrenergic G protein-coupled receptor. *Science* **318**, 1258-1265.

Cherezov, V. (2011). Lipidic cubic phase technologies for membrane protein structural studies. *Curr Opin Struct Biol* **21**, 559-566.

Cho, H.S., Dashdorj, N., Schotte, F., Graber, T., Henning, R., and Anfinrud, P. (2010). Protein structural dynamics in solution unveiled via 100-ps time-resolved x-ray scattering. *Proc Natl Acad Sci USA* **107**, 7281-7286.

Cho, H.S., Schotte, F., Dashdorj, N., Kyndt, J., and Anfinrud, P.A. (2013). Probing anisotropic structure changes in proteins with picosecond time-resolved small-angle X-ray scattering. *J Phys Chem B* **117**, 15825-15832.

Choi, J., Jung, Y.O., Lee, J.H., Yang, C., Kim, B., and Ihee, H. (2008). Folding dynamics of ferrocytochrome c in a denaturant-free environment probed by transient grating spectroscopy. *Chemphyschem* **9**, 2708-2714.

Choi, J., Muniyappan, S., Wallis, J.T., Royer, W.E., and Ihee, H. (2010). Protein Conformational Dynamics of Homodimeric Hemoglobin Revealed by Combined Time-Resolved Spectroscopic Probes. *Chemphyschem* **11**, 109-114.

Cohen, A.E., Soltis, S.M., Gonzalez, A., Aguila, L., Alonso-Mori, R., Barnes, C.O., Baxter, E.L., Brehmer, W., Brewster, A.S., Brunger, A.T., Calero, G., Chang, J.F., Chollet, M., Ehrensberger, P., Eriksson, T.L., et al. (2014). Goniometer-based femtosecond crystallography with X-ray free electron lasers. *Proc Natl Acad Sci USA* **111**, 17122-17127.

Coquelle, N., Brewster, A.S., Kapp, U., Shilova, A., Weinhausen, B., Burghammer, M., and Colletier, J.P. (2015). Raster-scanning serial protein crystallography using micro- and nano-focused synchrotron beams. *Acta Crystallogr D Biol Crystallogr* **71**, 1184-1196.

Demirci, H., Sierra, R.G., Laksmono, H., Shoeman, R.L., Botha, S., Barends, T.R., Nass, K., Schlichting, I., Doak, R.B., Gati, C., Williams, G.J., Boutet, S., Messerschmidt, M., Jogl, G., Dahlberg, A.E., et al. (2013). Serial femtosecond X-ray diffraction of 30S ribosomal subunit microcrystals in liquid suspension at ambient temperature using an X-ray free-electron laser. *Acta Crystallogr Sect F Struct Biol Cryst Commun* **69**, 1066-1069.

Dhouib, K., Malek, C.K., Pfleging, W., Gauthier-Manuel, B., Duffait, R., Thuillier, G., Ferrigno, R., Jacquamet, L., Ohana, J., Ferrer, J.L., Theobald-Dietrich, A., Giege, R., Lorber, B., and Sauter, C. (2009). Microfluidic chips for the crystallization of biomacromolecules by counter-diffusion and on-chip crystal X-ray analysis. *Lab Chip* **9**, 1412-1421.

Doniach, S. (1996). Studies of the structure of matter with photons from an X-ray free-electron laser. *J Synchrotron Radiat* **3**, 260-267.

Duss, O., Yulikov, M., Jeschke, G., and Allain, F.H. (2014). EPR-aided approach for solution structure determination of large RNAs or protein-RNA complexes. *Nat Commun* **5**, 3669-3677.

Elmlund, D., and Elmlund, H. (2015). Cryogenic electron microscopy and single-particle analysis. *Annu Rev Biochem* **84**, 499-517.

Emma, P., Akre, R., Arthur, J., Bionta, R., Bostedt, C., Bozek, J., Brachmann, A., Bucksbaum, P., Coffee, R., Decker, F.J., Ding, Y., Dowell, D., Edstrom, S., Fisher, A., Frisch, J., et al. (2010). First lasing and operation of an angstrom-wavelength free-electron laser. *Nat Photonics* **4**, 641-647.

Faham, S., and Bowie, J.U. (2002). Bicelle crystallization: a new method for crystallizing membrane proteins yields a monomeric bacteriorhodopsin structure. *J Mol Biol* **316**, 1-6.

Foucar, L., Barty, A., Coppola, N., Hartmann, R., Holl, P., Hoppe, U., Kassemeyer, S., Kimmel, N., Kupper, J., Scholz, M., Techert, S., White, T.A., Struder, L., and Ullrich, J. (2012). CASS-CFEL-ASG software suite. *Comput Phys Commun* **183**, 2207-2213.

Gati, C., Bourenkov, G., Klinge, M., Rehders, D., Stellato, F., Oberthur, D., Yefanov, O., Sommer, B.P., Mogk, S., Duszenko, M., Betzel, C., Schneider, T.R., Chapman, H.N., and Redecke, L. (2014). Serial crystallography on in vivo grown microcrystals using synchrotron radiation. *IUCrJ* **1**, 87-94.

Genick, U.K., Borgstahl, G.E.O., Ng, K., Ren, Z., Pradervand, C., Burke, P.M., Srajer, V., Teng, T.Y., Schildkamp, W., McRee, D.E., Moffat, K., and Getzoff, E.D. (1997). Structure of a protein photocycle intermediate by millisecond time-resolved crystallography. *Science* **275**, 1471-1475.

Gerdts, C.J., Elliott, M., Lovell, S., Mixon, M.B., Napuli, A.J., Staker, B.L., Nollert, P., and Stewart, L. (2008). The plug-based nanovolume Microcapillary Protein Crystallization System (MPCS). *Acta Crystallogr D* **64**, 1116-1122.

Ghosh, E., Kumari, P., Jaiman, D., and Shukla, A.K. (2015). Methodological advances: the unsung heroes of the GPCR structural revolution. *Nat Rev Mol Cell Bio* **16**, 69-81.

Gobl, C., Madl, T., Simon, B., and Sattler, M. (2014). NMR approaches for structural analysis of multidomain proteins and complexes in solution. *Prog Nucl Mag Res Sp* **80**, 26-63.

Graewert, M.A., and Svergun, D.I. (2013). Impact and progress in small and wide angle X-ray scattering (SAXS and WAXS). *Curr Opin Struct Biol* **23**, 748-754.

Guha, S., Perry, S.L., Pawate, A.S., and Kenis, P.J. (2012). Fabrication of

X-ray compatible microfluidic platforms for protein crystallization. *Sens Actuators B Chem* **174**, 1-9.

Guha, S., Perry, S.L., Pawate, A.S., and Kenis, P.J. (2012). Fabrication of X-ray compatible microfluidic platforms for protein crystallization. *Sens Actuators B Chem* **174**, 1-9.

Hattne, J., Echols, N., Tran, R., Kern, J., Gildea, R.J., Brewster, A.S., Alonso-Mori, R., Glockner, C., Hellmich, J., Laksmono, H., Sierra, R.G., Lassalle-Kaiser, B., Lampe, A., Han, G., Gul, S., et al. (2014). Accurate macromolecular structures using minimal measurements from X-ray free-electron lasers. *Nat Methods* **11**, 545-548.

Heymann, M., Opthalage, A., Wierman, J.L., Akella, S., Szebenyi, D.M., Gruner, S.M., and Fraden, S. (2014). Room-temperature serial crystallography using a kinetically optimized microfluidic device for protein crystallization and on-chip X-ray diffraction. *IUCrJ* **1**, 349-360.

Hirata, K., Shinzawa-Itoh, K., Yano, N., Takemura, S., Kato, K., Hatanaka, M., Muramoto, K., Kawahara, T., Tsukihara, T., Yamashita, E., Tono, K., Ueno, G., Hikima, T., Murakami, H., Inubushi, Y., et al. (2014). Determination of damage-free crystal structure of an X-ray-sensitive protein using an XFEL. *Nat Methods* **11**, 734-U174.

Hunter, M.S., Segelke, B., Messerschmidt, M., Williams, G.J., Zatsepin, N.A., Barty, A., Benner, W.H., Carlson, D.B., Coleman, M., Graf, A., Hau-Riege, S.P., Pardini, T., Seibert, M.M., Evans, J., Boutet, S., et al. (2014). Fixed-target protein serial microcrystallography with an x-ray free electron laser. *Sci Rep* **4**, 6026.

Ihee, H., Rajagopal, S., Srajer, V., Pahl, R., Anderson, S., Schmidt, M., Schotte, F., Anfinrud, P.A., Wulff, M., and Moffat, K. (2005). Visualizing reaction pathways in photoactive yellow protein from nanoseconds to seconds. *Proc Natl Acad Sci USA* **102**, 7145-7150.

Ihee, H. (2009). Visualizing solution-phase reaction dynamics with time-resolved X-ray liquidography. *Acc Chem Res* **42**, 356-366.

Ihee, H., Wulff, M., Kim, J., and Adachi, S. (2010). Ultrafast X-ray scattering: structural dynamics from diatomic to protein molecules. *Int Rev Phys Chem* **29**, 453-520.

Ishikawa, T., Aoyagi, H., Asaka, T., Asano, Y., Azumi, N., Bizen, T., Ego, H., Fukami, K., Fukui, T., Furukawa, Y., Goto, S., Hanaki, H., Hara, T., Hasegawa, T., Hatsui, T., et al. (2012). A compact X-ray free-electron laser emitting in the sub-angstrom region. *Nat Photonics* **6**, 540-544.

Jaskolski, M., Dauter, Z., and Wlodawer, A. (2014). A brief history of macromolecular crystallography, illustrated by a family tree and its Nobel fruits. *Febs J* **281**, 3985-4009.

Johansson, L.C., Arnlund, D., Katona, G., White, T.A., Barty, A., DePonte, D.P., Shoeman, R.L., Wickstrand, C., Sharma, A., Williams, G.J., Aquila, A., Bogan, M.J., Caleman, C., Davidsson, J., Doak, R.B., et al. (2013). Structure of a photosynthetic reaction centre determined by serial femtosecond crystallography. *Nat Commun* **4**, 2911.

Jung, Y.O., Lee, J.H., Kim, J., Schmidt, M., Moffat, K., Srajer, V., and Ihee, H. (2013). Volume-conserving trans-cis isomerization pathways in photoactive yellow protein visualized by picosecond X-ray crystallography. *Nat Chem* **5**, 212-220.

Kabsch, W. (2014). Processing of X-ray snapshots from crystals in random orientations. *Acta Crystallogr D* **70**, 2204-2216.

Kern, J., Alonso-Mori, R., Hellmich, J., Tran, R., Hattne, J., Laksmono, H., Glockner, C., Echols, N., Sierra, R.G., Sellberg, J., Lassalle-Kaiser, B., Gildea, R.J., Glatzel, P., Grosse-Kunstleve, R.W., Latimer, M.J., et al. (2012). Room temperature femtosecond X-ray diffraction of photosystem II microcrystals. *Proc Natl Acad Sci USA* **109**, 9721-9726.

Kern, J., Alonso-Mori, R., Tran, R., Hattne, J., Gildea, R.J., Echols, N., Glockner, C., Hellmich, J., Laksmono, H., Sierra, R.G., Lassalle-Kaiser, B., Koroidov, S., Lampe, A., Han, G.Y., Gul, S., et al. (2013). Simultaneous Femtosecond X-ray Spectroscopy and Diffraction of Photosystem II at Room Temperature. *Science* **340**, 491-495.

Khvostichenko, D.S., Schieferstein, J.M., Pawate, A.S., Laible, P.D., and Kenis, P.J. (2014). X-ray Transparent Microfluidic Chip for Mesophase-Based Crystallization of Membrane Proteins and On-Chip Structure Determination. *Cryst Growth Des* **14**, 4886-4890.

Kim, J., Lee, J.H., Kim, J., Jun, S., King, K.H., Kim, T.W., Wulff, M., and Ihee, H. (2012). Structural dynamics of 1,2-diiodoethane in cyclohexane probed by picosecond X-ray liquidography. *J Phys Chem A* **116**, 2713-2722.

Kim, K.H., Oang, K.Y., Kim, J., Lee, J.H., Kim, Y., and Ihee, H. (2011). Direct observation of myoglobin structural dynamics from 100 picoseconds to 1 microsecond with picosecond X-ray solution scattering. *Chem Commun (Camb)* **47**, 289-291.

Kim, K.H., Muniyappan, S., Oang, K.Y., Kim, J.G., Nozawa, S., Sato, T., Koshihara, S. Y., Henning, R., Kosheleva, I., Ki, H., Kim, T.W., Kim, J., Adachi, S., and Ihee, H. (2012). Direct observation of cooperative protein structural dynamics of homodimeric hemoglobin from 100 ps to 10 ms with pump-probe X-ray solution scattering. *J Am Chem Soc* **134**, 7001-7008.

Kim, K.H., Ki, H., Oang, K.Y., Nozawa, S., Sato, T., Kim, J., Kim, T.K., Kim, J., Adachi, S., and Ihee, H. (2013). Global reaction pathways in the photodissociation of I-3(-) ions in solution at 267 and 400 nm studied by picosecond X-ray liquidography. *Chemphyschem* **14**, 3687-3697.

Kim, K.H., Lee, J.H., Kim, J., Nozawa, S., Sato, T., Tomita, A., Ichiyanagi, K., Ki, H., Kim, J., Adachi, S., and Ihee, H. (2013). Solvent-dependent molecular structure of ionic species directly measured by ultrafast X-ray solution scattering. *Phys Rev Lett* **110**, 165505.

Kim, K.H., Ki, H., Lee, J.H., Park, S., Kong, Q., Kim, J., Kim, J., Wulff, M., and Ihee, H. (2015). Solvent-dependent structure of molecular iodine probed by picosecond X-ray solution scattering. *Phys Chem Chem Phys* **17**, 8633-8637.

Kim, K.H., Kim, J.G., Nozawa, S., Sato, T., Oang, K.Y., Kim, T., Ki, H., Jo, J., Park, S., Song, C., Sato, T., Ogawa, K., Togashi, T., Tono, K., Yabashi, M., et al. (2015). Direct observation of bond formation in solution with femtosecond X-ray scattering. *Nature* **518**, 385-389.

Kim, T.K., Lee, J.H., Wulff, M., Kong, Q.Y., and Ihee, H. (2009). Spatiotemporal kinetics in solution studied by time-resolved X-ray liquidography (solution scattering). *Chemphyschem* **10**, 1958-1980.

Kim, T.W., Lee, J.H., Choi, J., Kim, K.H., van Wilderen, L.J., Guerin, L., Kim, Y., Jung, Y. O., Yang, C., Kim, J., Wulff, M., van Thor, J.J., and Ihee, H. (2012). Protein structural dynamics of photoactive yellow protein in solution revealed by pump-probe X-ray solution scattering. *J Am Chem Soc* **134**, 3145-3153.

Kim, T.W., Kim, J.G., Yang, C., Ki, H., Jo, J., and Ihee, H. (2014). Pump-Probe X-ray Solution Scattering Reveals Accelerated Folding of Cytochrome c Upon Suppression of Misligation. *Bull Korean Chem Soc* **35**, 695-696.

Kisselman, G., Qiu, W., Romanov, V., Thompson, C.M., Lam, R., Battaile, K.P., Pai, E. F., and Chirgadze, N.Y. (2011). X-CHIP: an integrated platform for high-throughput protein crystallization and on-the-chip X-ray diffraction data collection. *Acta Crystallogr D* **67**, 533-539.

Knapp, J.E., Pahl, R., Srajer, V., and Royer, W.E. (2006). Allosteric action in real time: Time-resolved crystallographic studies of a cooperative dimeric hemoglobin. *Proc Natl Acad Sci USA* **103**, 7649-7654.

Konermann, L., Pan, J.X., and Liu, Y.H. (2011). Hydrogen exchange mass spectrometry for studying protein structure and dynamics. *Chem Soc Rev* **40**, 1224-1234.

Kong, Q.Y., Kim, J., Lorenc, M., Kim, T.K., Ihee, H., and Wulff, M. (2005). Photodissociation reaction of 1,2-diiodoethane in solution: A theoretical and X-ray diffraction study. *J Phys Chem A* **109**, 10451-10458.

Kong, Q.Y., Lee, J.H., Plech, A., Wulff, M., Ihee, H., and Koch, M.H.J. (2008). Ultrafast X-ray solution scattering reveals an unknown reaction intermediate in the photolysis of [Ru-3(CO)(12)]. *Angew Chem Int Edit* **47**, 5550-5553.

Kong, Q.Y., Lee, J.H., Lo Russo, M., Kim, T.K., Lorenc, M., Cammarata, M., Bratos, S., Buslaps, T., Honkimaki, V., Ihee, H., and Wulff, M. (2010). Photolysis of Br-2 in CCl4 studied by time-resolved X-ray scattering. *Acta Crystallogr A* **66**, 252-260.

Koopmann, R., Cupelli, K., Redecke, L., Nass, K., Deponte, D.P., White, T.A., Stellato, F., Rehders, D., Liang, M., Andreasson, J., Aquila, A., Bajt, S., Barthelmess, M., Barty, A., Bogan, M.J., et al. (2012). In vivo protein crystallization opens new routes in structural biology. *Nat Methods* **9**, 259-262.

Kupitz, C., Basu, S., Grotjohann, I., Fromme, R., Zatsepin, N.A., Rendek, K.N., Hunter, M.S., Shoeman, R.L., White, T.A., Wang, D., James, D., Yang, J.H., Cobb, D. E., Reeder, B., Sierra, R.G., et al. (2014). Serial time-resolved crystallography of photosystem II using a femtosecond X-ray laser. *Nature* **513**, 261-265.

Kupitz, C., Grotjohann, I., Conrad, C.E., Roy-Chowdhury, S., Fromme, R., and Fromme, P. (2014). Microcrystallization techniques for serial femtosecond crystallography using photosystem II from Thermosynechococcus elongatus as a model system. *Philos Trans R Soc Lond B Biol Sci* **369**, 20130316.

Lee, J.H., Wulff, M., Bratos, S., Petersen, J., Guerin, L., Leicknam, J.C., Carnmarata, M., Kong, Q., Kim, J., Moller, K.B., and Ihee, H. (2013). Filming the birth of molecules and accompanying solvent rearrangement. *J Am Chem Soc* **135**, 3255-3261.

Lemke, H.T., Bressler, C., Chen, L.X., Fritz, D.M., Gaffney, K.J., Galler, A., Gawelda, W., Haldrup, K., Hartsock, R.W., Ihee, H., Kim, J., Kim, K.H., Lee, J.H., Nielsen, M. M., Stickrath, A.B., et al. (2013). Femtosecond X-ray absorption spectroscopy at a hard X-ray free electron laser: application to spin crossover dynamics. *J Phys Chem A* **117**, 735-740.

Levantino, M., Schiro, G., Lemke, H.T., Cottone, G., Glownia, J.M., Zhu, D., Chollet, M., Ihee, H., Cupane, A., and Cammarata, M. (2015). Ultrafast myoglobin structural dynamics observed with an X-ray free-electron laser. *Nat Commun* **6**, 6772.

Liu, H., and Spence, J.C. (2014). The indexing ambiguity in serial femtosecond crystallography (SFX) resolved using an expectation maximization algorithm. *IUCrJ* **1**, 393-401.

Liu, W., Wacker, D., Gati, C., Han, G.W., James, D., Wang, D., Nelson, G., Weierstall, U., Katritch, V., Barty, A., Zatsepin, N.A., Li, D., Messerschmidt, M., Boutet, S., Williams, G.J., et al. (2013). Serial femtosecond crystallography of G protein-coupled receptors. *Science* **342**, 1521-1524.

Liu, W., Wacker, D., Wang, C., Abola, E., and Cherezov, V. (2014). Femtosecond crystallography of membrane proteins in the lipidic cubic phase. *Philos Trans R Soc Lond B Biol Sci* **369**, 20130314.

Lomb, L., Steinbrener, J., Bari, S., Beisel, D., Berndt, D., Kieser, C., Lukat, M., Neef, N., and Shoeman, R.L. (2012). An anti-settling sample delivery instrument for serial femtosecond crystallography. *J Appl Cryst* **45**, 674-678.

Lopez, C.J., Fleissner, M.R., Brooks, E.K., and Hubbell, W.L. (2014). Stationary-phase EPR for exploring protein structure, conformation, and dynamics in spin-labeled proteins. *Biochemistry* **53**, 7067-7075.

Lyubimov, A.Y., Murray, T.D., Koehl, A., Araci, I.E., Uervirojnangkoorn, M., Zeldin, O.B., Cohen, A.E., Soltis, S.M., Baxter, E.L., Brewster, A.S., Sauter, N.K., Brunger, A.T., and Berger, JM. (2015). Capture and X-ray diffraction studies of protein microcrystals in a microfluidic trap array. *Acta Crystallogr D* **71**, 928-940.

Malkin, A.J., and Thorne, R.E. (2004). Growth and disorder of macromolecular crystals: insights from atomic force microscopy and X-ray diffraction studies. *Methods* **34**, 273-299.

Malmerberg, E., Omran, Z., Hub, J.S., Li, X.W., Katona, G., Westenhoff, S., Johansson, L.C., Andersson, M., Cammarata, M., Wulff, M., van der Spoel, D., Davidsson, J., Specht, A., and Neutze, R. (2011). Time-resolved WAXS reveals accelerated conformational changes in iodoretinal-substituted proteorhodopsin. *Biophys J* **101**, 1345-1353.

Mchaourab, H.S., Steed, P.R., and Kazmier, K. (2011). Toward the fourth dimension of membrane protein structure: insight into dynamics from spin-labeling EPR spectroscopy. *Structure* **19**, 1549-1561.

Mertens, H.D.T., and Svergun, D.I. (2010). Structural characterization of proteins and complexes using small-angle X-ray solution scattering. *J Struct Biol* **172**, 128-141.

Misquitta, L.V., Misquitta, Y., Cherezov, V., Slattery, O., Mohan, J.M., Hart, D., Zhalnina, M., Cramer, W.A., and Caffrey, M. (2004). Membrane protein crystallization in lipidic mesophases with tailored bilayers. *Structure* **12**, 2113-2124.

Neutze, R., Wouts, R., van der Spoel, D., Weckert, E., and Hajdu, J. (2000). Potential for biomolecular imaging with femtosecond X-ray pulses. *Nature* **406**, 752-757.

Ng, K., Ren, Z., Moffat, K., Borgstahl, G.E.O., Mcree, D.E., and Getzoff, E.D. (1993). Time-Resolved Photochemical Studies of Photoactive Yellow Protein (Pyp) Crystals. *Biophys J* **64**, A373-A373.

Nogly, P., James, D., Wang, D., White, T.A., Zatsepin, N., Shilova, A., Nelson, G., Liu, H., Johansson, L., Heymann, M., Jaeger, K., Metz, M., Wickstrand, C., Wu, W., Bath, P., et al. (2015). Lipidic cubic phase serial millisecond crystallography using synchrotron radiation. *IUCrJ* **2**, 168-176.

Oang, K.Y., Kim, J.G., Yang, C., Kim, T.W., Kim, Y., Kim, K.H., Kim, J.,

and Ihee, H. (2014). Conformational Substates of Myoglobin Intermediate Resolved by Picosecond X-ray Solution Scattering. *J Phys Chem Lett* **5**, 804-808.

Oang, K.Y., Kim, K.H., Jo, J., Kim, Y.M., Kim, J.G., Kim, T.W., Jun, S., Kim, J., and Ihee, H. (2014). Sub-100-ps structural dynamics of horse heart myoglobin probed by time-resolved X-ray solution scattering. *Chem Phys* **442**, 137-142.

Ogata, H., and Lubitz, W. (2014). Protein crystallography using free-electron lasers: water oxidation in photosynthesis. *Angew Chem Int Ed Engl* **53**, 13007-13008.

Osawa, M., Takeuchi, K., Ueda, T., Nishida, N., and Shimada, I. (2012). Functional dynamics of proteins revealed by solution NMR. *Curr Opin Struct Biol* **22**, 660-669.

PebayPeyroula, E., Rummel, G., Rosenbusch, J.P., and Landau, E.M. (1997). X-ray structure of bacteriorhodopsin at 2.5 angstroms from microcrystals grown in lipidic cubic phases. *Science* **277**, 1676-1681.

Petoukhov, M.V., and Svergun, D.I. (2013). Applications of small-angle X-ray scattering to biomacromolecular solutions. *Int J Biochem Cell Biol* **45**, 429-437.

Ramachandran, P.L., Lovett, J.E., Carl, P.J., Cammarata, M., Lee, J.H., Jung, Y.O., Ihee, H., Timmel, C.R., and van Thor, J.J. (2011). The short-lived signaling state of the photoactive yellow protein photoreceptor revealed by combined structural probes. *J Am Chem Soc* **133**, 9395-9404.

Rasmussen, S.G.F., Choi, H.J., Rosenbaum, D.M., Kobilka, T.S., Thian, F.S., Edwards, P.C., Burghammer, M., Ratnala, V.R.P., Sanishvili, R., Fischetti, R.F., Schertler, G.F.X., Weis, W.I., and Kobilka, B.K. (2007). Crystal structure of the human beta(2) adrenergic G-protein-coupled receptor. *Nature* **450**, 383-U384.

Redecke, L., Nass, K., DePonte, D.P., White, T.A., Rehders, D., Barty, A., Stellato, F., Liang, M., Barends, T.R., Boutet, S., Williams, G.J., Messerschmidt, M., Seibert, M.M., Aquila, A., Arnlund, D., et al. (2013). Natively inhibited Trypanosoma brucei cathepsin B structure determined by using an X-ray laser. *Science* **339**, 227-230.

Redecke, L., Nass, K., DePonte, D.P., White, T.A., Rehders, D., Barty, A., Stellato, F., Liang, M.N., Barends, T.R.M., Boutet, S., Williams, G.J., Messerschmidt, M., Seibert, M.M., Aquila, A., Arnlund, D., et al. (2013). Natively inhibited trypanosoma brucei cathepsin B structure determined by using an X-ray laser. *Science* **339**, 227-230.

Richardson, J.S., and Richardson, D.C. (2014). Biophysical highlights from 54 years of macromolecular crystallography. *Biophys J* **106**, 510-525.

Rossmann, M.G. (2014). Serial crystallography using synchrotron radiation. *IUCrJ* **1**, 84-86.

Sauter, C., Dhouib, K., and Lorber, B. (2007). From macrofluidics to microfluidics for the crystallization of biological macromolecules. *Cryst Growth Des* **7**, 2247-2250.

Sawaya, M.R., Cascio, D., Gingery, M., Rodriguez, J., Goldschmidt, L., Colletier, J.P., Messerschmidt, M.M., Boutet, S., Koglin, J.E., Williams, G.J., Brewster, A.S., Nass, K., Hattne, J., Botha, S., Doak, R.B., et al. (2014). Protein crystal structure obtained at 2.9 Å resolution from injecting bacterial cells into an X-ray free-electron laser beam. *Proc Natl Acad Sci USA* **111**, 12769-12774.

Schmidt, M., Pahl, R., Srajer, V., Anderson, S., Ren, Z., Ihee, H., Rajagopal, S., and Moffat, K. (2004). Protein kinetics: Structures of intermediates and reaction mechanism from time-resolved x-ray data. *Proc Natl Acad Sci USA* **101**, 4799-4804.

Schmidt, M., Ihee, H., Pahl, R., and Srajer, V. (2005). Protein-ligand interaction probed by time-resolved crystallography. *Methods Mol Biol* **305**, 115-154.

Schmidt, M. (2013). Mix and Inject: Reaction Initiation by Diffusion for Time-Resolved Macromolecular Crystallography. *Adv Cond Matter Phys* **2013**, Article ID 167276.

Schotte, F., Cho, H.S., Kaila, V.R.I., Kamikubo, H., Dashdorj, N., Henry, E.R., Graber, T.J., Henning, R., Wulff, M., Hummer, G., Kataoka, M., and Anfinrud, P.A. (2012). Watching a signaling protein function in real time via 100-ps time-resolved Laue crystallography. *Proc Natl Acad Sci USA* **109**, 19256-19261.

Schroer, C.G., Kurapova, O., Patommel, J., Boye, P., Feldkamp, J., Lengeler, B., Burghammer, M., Riekel, C., Vincze, L., van der Hart, A., and Kuchler, M. (2005). Hard x-ray nanoprobe based on refractive x-ray lenses.

*Appl Phys Lett* **87**.

Shi, Y. (2014). A glimpse of structural biology through X-ray crystallography. *Cell* **159**, 995-1014.

Sierra, R.G., Laksmono, H., Kern, J., Tran, R., Hattne, J., Alonso-Mori, R., Lassalle-Kaiser, B., Glockner, C., Hellmich, J., Schafer, D.W., Echols, N., Gildea, R.J., Grosse-Kunstleve, R.W., Sellberg, J., McQueen, T.A., et al. (2012). Nanoflow electrospinning serial femtosecond crystallography. *Acta Crystallogr D Biol Crystallogr* **68**, 1584-1587.

Son, S.K., Chapman, H.N., and Santra, R. (2011). Multiwavelength anomalous diffraction at high X-ray intensity. *Phys Rev Lett* **107**, 218102.

Son, S.K., Chapman, H.N., and Santra, R. (2013). Determination of multiwavelength anomalous diffraction coefficients at high x-ray intensity. *J Phys B-at Mol Opt* **46**, 164015.

Spence, J.C.H., and Doak, R.B. (2004). Single molecule diffraction. *Phys Rev Lett* **92**.

Srajer, V., Teng, T.Y., Ursby, T., Pradervand, C., Ren, Z., Adachi, S., Schildkamp, W., Bourgeois, D., Wulff, M., and Moffat, K. (1996). Photolysis of the carbon monoxide complex of myoglobin: Nanosecond time-resolved crystallography. *Science* **274**, 1726-1729.

Srajer, V., Ren, Z., Teng, T.Y., Schmidt, M., Ursby, T., Bourgeois, D., Pradervand, C., Schildkamp, W., Wulff, M., and Moffat, K. (2001). Protein conformational relaxation and ligand migration in myoglobin: A nanosecond to millisecond molecular movie from time-resolved Laue X-ray diffraction. *Biochemistry* **40**, 13802-13815.

Stellato, F., Oberthur, D., Liang, M., Bean, R., Gati, C., Yefanov, O., Barty, A., Burkhardt, A., Fischer, P., Galli, L., Kirian, R.A., Meyer, J., Panneerselvam, S., Yoon, C.H., Chervinskii, F., et al. (2014). Room-temperature macromolecular serial crystallography using synchrotron radiation. *IUCrJ* **1**, 204-212.

Sugahara, M., Mizohata, E., Nango, E., Suzuki, M., Tanaka, T., Masuda, T., Tanaka, R., Shimamura, T., Tanaka, Y., Suno, C., Ihara, K., Pan, D., Kakinouchi, K., Sugiyama, S., Murata, M., et al. (2015). Grease matrix as a versatile carrier of proteins for serial crystallography. *Nat Methods* **12**, 61-63.

Tenboer, J., Basu, S., Zatsepin, N., Pande, K., Milathianaki, D., Frank, M., Hunter, M., Boutet, S., Williams, G.J., Koglin, J.E., Oberthuer, D., Heymann, M., Kupitz, C., Conrad, C., Coe, J., et al. (2014). Time-resolved serial crystallography captures high-resolution intermediates of photoactive yellow protein. *Science* **346**, 1242-1246.

Tono, K., Nango, E., Sugahara, M., Song, C., Park, J., Tanaka, T., Tanaka, R., Joti, Y., Kameshima, T., Ono, S., Hatsui, T., Mizohata, E., Suzuki, M., Shimamura, T., Tanaka, Y., et al. (2015). Diverse application platform for hard X-ray diffraction in SACLA (DAPHNIS): application to serial protein crystallography using an X-ray free-electron laser. *J Synchrotron Radiat* **22**, 532-537.

Torchia, D.A. (2015). NMR studies of dynamic biomolecular conformational ensembles. *Prog Nucl Mag Res Sp* **84**, 14-32.

Tusnady, G.E., Dosztanyi, Z., and Simon, I. (2004). Transmembrane proteins in the Protein Data Bank: identification and classification. *Bioinformatics* **20**, 2964-2972.

Venkatakrishnan, A.J., Deupi, X., Lebon, G., Tate, C.G., Schertler, G.F., and Babu, M.M. (2013). Molecular signatures of G-protein-coupled receptors. *Nature* **494**, 185-194.

Wadsten, P., Wohri, A.B., Snijder, A., Katona, G., Gardiner, A.T., Cogdell, R.J., Neutze, R., and Engstrom, S. (2006). Lipidic sponge phase crystallization of membrane proteins. *J Mol Biol* **364**, 44-53.

Walzthoeni, T., Leitner, A., Stengel, F., and Aebersold, R. (2013). Mass spectrometry supported determination of protein complex structure. *Curr Opin Struct Biol* **23**, 252-260.

Wang, D.J., Weierstall, U., Pollack, L., and Spence, J. (2014). Double-focusing mixing jet for XFEL study of chemical kinetics. *J Synchrotron Radiat* **21**, 1364-1366.

Weierstall, U., Spence, J.C., and Doak, R.B. (2012). Injector for scattering measurements on fully solvated biospecies. *Rev Sci Instrum* **83**, 035108.

Weierstall, U., James, D., Wang, C., White, T.A., Wang, D., Liu, W., Spence, J.C., Bruce Doak, R., Nelson, G., Fromme, P., Fromme, R., Grotjohann, I., Kupitz, C., Zatsepin, N.A., Liu, H., et al. (2014). Lipidic cubic phase injector facilitates membrane protein serial femtosecond crystallography. *Nat Commun* **5**, 3309.

White, T.A., Kirian, R.A., Martin, A.V., Aquila, A., Nass, K., Barty, A., and Chapman, H.N. (2012). CrystFEL: a software suite for snapshot serial crystallography. *J Appl Crystallogr* **45**, 335-341.

White, T.A., Barty, A., Stellato, F., Holton, J.M., Kirian, R.A., Zatsepin, N.A., and Chapman, H.N. (2013). Crystallographic data processing for free-electron laser sources. *Acta Crystallogr D* **69**, 1231-1240.

Wohri, A.B., Johansson, L.C., Wadsten-Hindrichsen, P., Wahlgren, W.Y., Fischer, G., Horsefield, R., Katona, G., Nyblom, M., Oberg, F., Young, G., Cogdell, R.J., Fraser, N.J., Engstrom, S., and Neutze, R. (2008). A lipidic-sponge phase screen for membrane protein crystallization. *Structure* **16**, 1003-1009.

Wohri, A.B., Wahlgren, W.Y., Malmerberg, E., Johansson, L.C., Neutze, R., and Katona, G. (2009). Lipidic Sponge Phase Crystal Structure of a Photosynthetic Reaction Center Reveals Lipids on the Protein Surface. *Biochemistry* **48**, 9831-9838.

Zhang, W.K., Alonso-Mori, R., Bergmann, U., Bressler, C., Chollet, M., Galler, A., Gawelda, W., Hadt, R.G., Hartsock, R.W., Kroll, T., Kjaer, K.S., Kubicek, K., Lemke, H.T., Liang, H.Y.W., Meyer, D.A., et al. (2014). Tracking excited-state charge and spin dynamics in iron coordination complexes. *Nature* **509**, 345-348.

Zhu, Y., Zhu, L.N., Guo, R., Cui, H.J., Ye, S., and Fang, Q. (2014). Nanoliter-scale protein crystallization and screening with a microfluidic droplet robot. *Sci Rep* **4**, 5046